PROCEEDINGS A

royalsocietypublishing.org/journal/rspa

Research

Cite this article: Wagner HNR, Hühne C, Khakimova R, Niemann S, Wang M, Zhang J. 2025 Structured chaos: redefining the design of buckling-critical cylindrical shells. *Proc. R. Soc. A* **481**: 20250196.
https://doi.org/10.1098/rspa.2025.0196

Received: 12 March 2025
Accepted: 21 July 2025

Subject Areas:
structural engineering, computational mechanics, statistics

Keywords:
knockdown factor, mechanistic design curve (MDC), shell buckling, Monte Carlo simulation, stability regime, imperfection sensitivity

Author for correspondence:
H. N. R. Wagner
e-mail: ro.wagner@tu-braunschweig.de

Structured chaos: redefining the design of buckling-critical cylindrical shells

H. N. R. Wagner[1], C. Hühne[1,2], R. Khakimova[1], S. Niemann[2], M. Wang[3] and J. Zhang[3]

[1]Technical University Braunschweig, Institute of Adaptronic and Functional Integration, Langer Kamp 6 Braunschweig 38106, Germany
[2]German Aerospace Center (DLR), Institute for Composite Structures and Adaptive Systems, Lilienthalplatz 7, Braunschweig 38108, Germany
[3]School of Mechanical Engineering, Jiangsu University of Science and Technology, Zhenjiang 212003, People's Republic of China

HNRW, 0000-0003-2749-1455

Experimental studies on axially compressed cylindrical shells have historically shown large variability in buckling loads, often challenging existing theoretical models. Our analysis reveals that this scatter follows a structured, regime-dependent trend—formalized here as the mechanistic design curve (MDC). This curve captures a systematic transition between three dominant failure mechanisms as a function of slenderness: global collapse (Regime 1), transitional recovery (Regime 2) and localized instability (Regime 3). Through large-scale Monte Carlo simulations incorporating measured geometric imperfections and localized buckling triggers, we demonstrate how buckling behaviour evolves across these regimes, exhibiting a characteristic dip–recovery–decline pattern in knockdown factors. The MDC framework is validated using decades of experimental data on both cylindrical and conical shells, revealing consistent regime boundaries despite variations in geometry and manufacturing quality. By unifying physics-based mechanisms with statistical robustness, the MDC replaces empirical lower-bound approaches

Electronic supplementary material is available online at https://doi.org/10.6084/m9.figshare.c.7987106.

THE ROYAL SOCIETY PUBLISHING

(e.g. NASA SP-8007) with predictive, regime-aware design rules. Case studies demonstrate weight savings exceeding 14%—and up to 31% in optimized configurations—while maintaining safety, highlighting the MDC's potential to transform lightweight shell design. This work reinterprets historical scatter and reveals that what appeared chaotic is, in fact, governed by hidden structure.

1. Introduction

Shell buckling is widely regarded as one of the most complex and perplexing problems in structural mechanics [1]. Buckling of cylinders [2] under axial compression occurs when a thin-walled cylindrical structure experiences a stability-driven loss of load-carrying capacity (figure 1), often at loads far below classical predictions. Classical linear theory [3] predicts the critical buckling load N_{theory} after equation (1.1) using a closed-form expression that depends on the cylinder's elastic modulus E, wall thickness t and the Poisson's ratio ν.

$$N_{\text{theory}} = \frac{2 \cdot \pi \cdot E \cdot t^2}{\sqrt{3(1-\nu^2)}}. \tag{1.1}$$

For decades, engineers and scientists have grappled with the significant discrepancies observed between theoretical predictions and experimental results. This divergence has limited the efficiency of structural designs and has contributed to the long-standing perception that shell buckling behaviour is chaotic and unpredictable—particularly when relevant imperfection signatures are unknown or cannot be fully characterized in practice.

One of the primary sources of uncertainty in shell buckling is its extreme sensitivity to small deviations from the ideal geometry, commonly referred to as geometric imperfections [4,5], figure 2. These imperfections arise from manufacturing processes, material inhomogeneities or in-service deformations, and they significantly influence the actual buckling strength of a shell. Unlike other structural failures that are primarily governed by material properties, shell buckling is heavily influenced by these deviations, leading to large reductions in load-carrying capacity.

Design guidelines, such as NASA SP-8007 [7] for cylindrical shells and NASA SP-8019 [8] for conical shells, provide empirical lower-bound estimates but fail to capture the underlying physics driving buckling behaviour. The result is an overly conservative approach that leads to excessive material use and limits structural efficiency in aerospace, automotive and civil engineering applications.

Figure 3 highlights the persistent mismatch between theory and experiment by presenting knockdown factors (KDFs), defined in equation (1.2) as the ratio of the measured buckling load N_{exp} to the theoretical prediction N_{theory}.

$$\text{KDF} = \frac{N_{\text{exp}}}{N_{\text{theory}}}. \tag{1.2}$$

Ideally, this ratio according to equation (1.2) should be close to 1, indicating that structures reach their full theoretical strength. However, experimental data reveal deviations exceeding 70%, highlighting the extreme imperfection sensitivity of shell buckling. Shell buckling design still predominantly relies on empirical KDFs derived from lower-bound curves, such as those provided by NASA SP-8007 from equation (1.3). These factors depend on the cylinder radius R to shell thickness t ratio R/t and are applied to the theoretical buckling load as a safety margin in structural design.

$$\text{KDF}_{\text{NASA}} = 1 - 0.902 \cdot \left(1 - e^{-(1/16\sqrt{R/t})}\right). \tag{1.3}$$

These empirical formulae, while widely used, do not capture the true complexity of shell stability, leading to overdesign. As a result, researchers have turned to more sophisticated numerical and probabilistic approaches to refine KDFs and enhance design predictions [10,11].

Figure 1. Cylindrical shells under axial compression: failure in service (left), laboratory test (right) from [2].

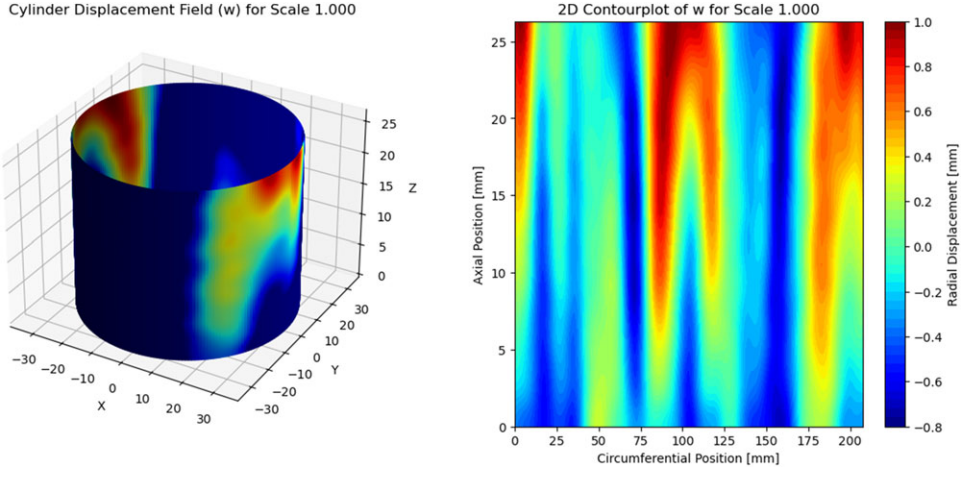

Figure 2. Three-dimensional representation of a cylindrical shell with an imperfection pattern applied (left). A contour plot of the imperfection pattern distribution along the shell surface from [6] (right).

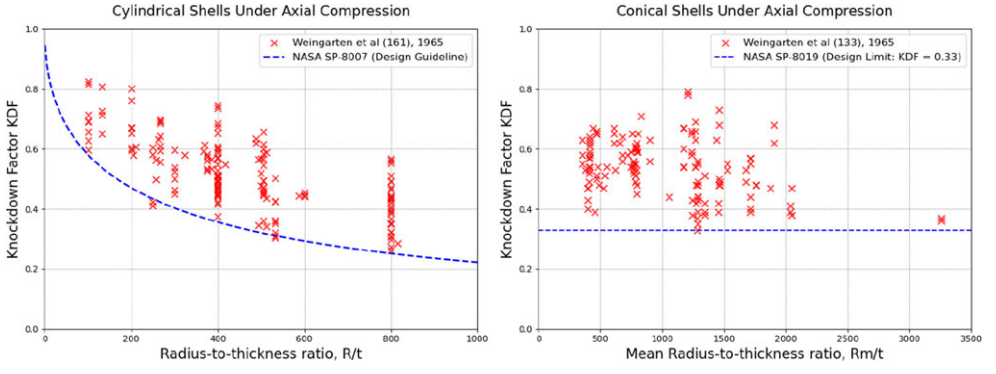

Figure 3. KDF versus *R/t* ratio: experimental data for cylindrical (left) and conical (right) shells under axial compression from [9] with NASA SP recommendations.

The predictive accuracy of shell buckling analysis has significantly improved with the advent of advanced computational tools. Finite element analysis, in particular, has become an indispensable method for studying thin-walled cylindrical shells subjected to axial compression [12]. These simulations are now capable of incorporating detailed imperfection fields—either obtained from experimental measurements or generated statistically—to assess their impact on structural stability [13–15].

Complementing deterministic approaches, probabilistic frameworks have been developed to model the inherent variability of geometric imperfections [16,17]. This has led to the concept of stochastic KDFs, which better capture the range of possible buckling responses in real-world structures [18].

Despite these advances in simulation, experimental validation remains a critical component of shell buckling research. Laboratory tests under controlled axial loading provide empirical data on both initial failure and post-buckling behaviour [19,20]. High-fidelity measurement techniques, such as digital image correlation, enable precise tracking of deformation fields and surface imperfections [21].

These experimental datasets are essential for calibrating computational models, especially with respect to the representation of initial imperfections [22,23]. By aligning simulated and observed buckling responses—including critical loads and mode shapes—researchers can refine their numerical models and improve their reliability for design applications [24,25].

Although theoretical frameworks such as Koiter's imperfection sensitivity theory have laid the foundation for understanding shell buckling, significant discrepancies between theory and test results persist in practice—particularly when imperfection data are incomplete or poorly characterized. Given the high cost and risk of structural failure, engineers often fall back on empirical design rules such as the NASA SP-8007 KDFs.

As emphasized in [26]: 'The need to use these empirical corrections is nevertheless deplorable for the theorists since it makes generalizations outside of the range of the existing experiments, and especially to different types of shells, uncertain'.

Rather than treating buckling strength as the outcome of a single dominant effect, this study reveals that the observed scatter in experimental data follows a structured pattern—governed by a continuous shift in the underlying failure mechanisms. This insight lays the foundation for a new generation of predictive methods in shell design: grounded in physical understanding, rather than historical correction factors.

2. Stability regimes in cylinder buckling

In recent years, several studies have proposed lower-bound KDF curves for cylindrical shells under axial compression [27,28], derived from localized buckling mechanisms in perfect geometries—typically plotted against the Batdorf parameter Z according to equation (2.1).

$$Z = \frac{L^2 \cdot \sqrt{(1 - \nu^2)}}{R \cdot t}. \tag{2.1}$$

These models, often based on perturbation [29] or reduced-stiffness concepts [30], have been successful in predicting the worst-case response of shells produced with high geometric precision—such as filament-wound composites or machined specimens. However, when applied to shells manufactured by rolling, welding or deep drawing (e.g. Mylar or metal sheets), these same models often significantly overpredict the buckling load, figure 4.

This discrepancy points to a deeper issue: the effectiveness of local-buckling-based models is not universally valid but rather depends on the type of manufacturing-specific geometric imperfection signatures [13].

To investigate this, we performed a large-scale probabilistic Monte Carlo (MC) analysis, systematically sampling combinations of measured geometric imperfections (MGIs) and localized buckling triggers, to replicate real-world manufacturing variability and capture worst-case stability behaviour.

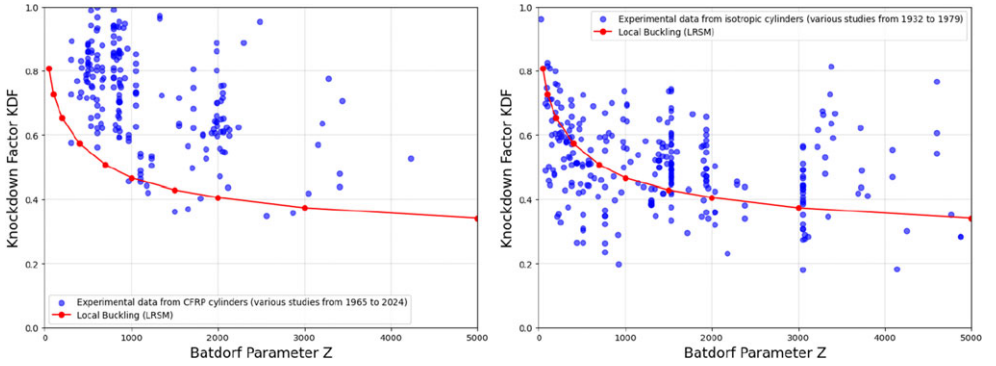

Figure 4. Comparison of experimental KDFs and local buckling predictions LRSM for different cylinder datasets: for 222 CFRP composite cylinders [31] (left), for 309 isotropic cylinders [32] (right).

A detailed description of the numerical model, imperfection database, MC set-up and convergence analysis can be found in the technical appendix A. These aspects were intentionally excluded here to maintain focus on the physical classification and regime interpretation.

(a) Introduction of mechanistic design curves

For nearly a century, the buckling behaviour of thin-walled cylindrical shells under axial compression has been interpreted through the lens of imperfection sensitivity—the principle that small geometric deviations drastically reduce load-carrying capacity. Koiter's imperfection sensitivity theory provides a rigorous asymptotic framework for this phenomenon, demonstrating how imperfections, particularly axisymmetric ones, lead to significant reductions in buckling loads. However, Koiter's theory assumes a universal sensitivity to imperfections and does not systematically address the transition between global and local buckling mechanisms across varying shell slenderness or manufacturing-induced imperfection patterns.

This study introduces the *mechanistic design curve* (*MDC*), a novel framework that reveals a structured, regime-dependent organization in shell buckling behaviour. Using a probabilistic MC framework combining MGIs with localized buckling mechanisms via the localized reduced stiffness method (LRSM), we uncover a non-monotonic trend in the 1% quantile of KDFs plotted against the Batdorf parameter Z, as shown in figure 5. This trend, termed the MDC, is characterized by a distinct dip, partial recovery and renewed decline in KDFs, reflecting a systematic shift in the dominant buckling trigger: from global imperfection-driven failures at low Z (Regime 1), through a transitional/recovery region (Regime 2), to localized buckling-driven failures at high Z (Regime 3). The MDC's non-monotonic behaviour, validated through thousands of MC simulations (see appendix Ad(ii)) and historical experimental data (figures 6–8), is not predicted by classical imperfection sensitivity theory and represents a new insight into the statistical structure of shell stability.

Figure 5 (left) illustrates this trend and enables the classification of shell behaviour into three distinct stability regimes, each defined by the dominant buckling trigger responsible for the worst-case scenario (i.e. the 1% quantile of the KDF distribution):

— Regime 1—low Z:
In this regime, the critical failure is triggered by global imperfection patterns—large-scale geometric deviations introduced by manufacturing processes such as welding, rolling or deep drawing. These imperfections govern the worst-case response, leading to significant scatter in KDFs. Localized buckling may occur in individual cases, but the lowest buckling loads are consistently associated with global imperfection-driven failures.

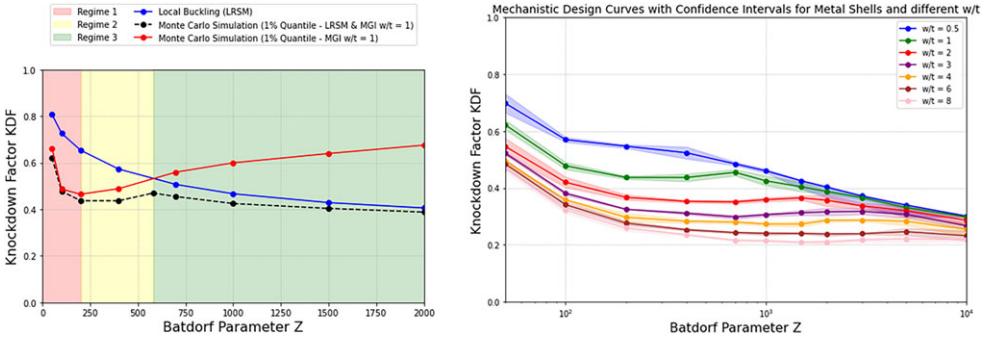

Figure 5. KDF versus Batdorf parameter Z, highlighting regime-dependent stability across three regimes (global, transition/recovery, local). Curves show 1% quantile results from MC simulations with/without LRSM triggers (black/red) and local buckling limit (blue), all for MGIs with imperfection amplitude-to-thickness ratio $w/t = 1$ (left), influence of increasing w/t ratio on stability regimes and KDF (right).

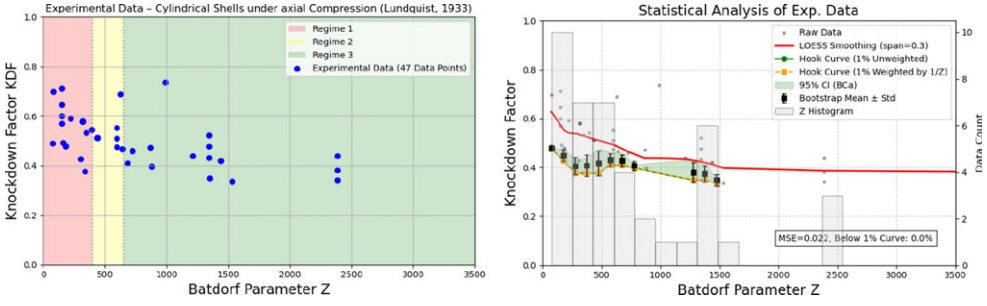

Figure 6. Left: cylindrical shell exp. KDFs from Lundquist [34] versus Z, coloured by stability regime. Right: different statistical metrics to analyse the exp. data. exp., experiment.

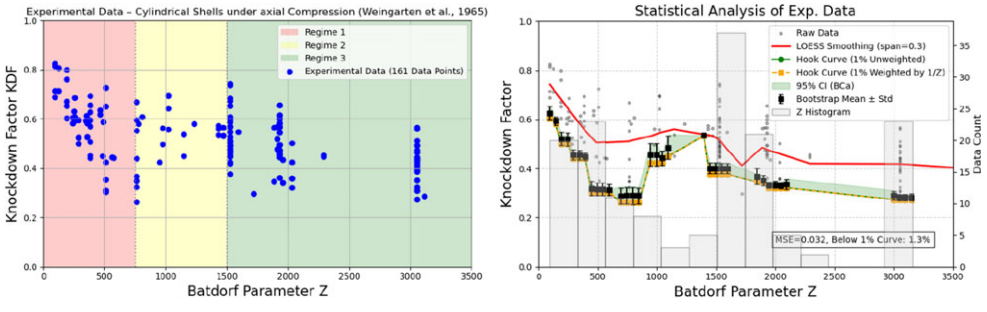

Figure 7. Left: cylindrical shell exp. KDFs from Weingarten *et al.* [9] versus Z, coloured by stability regime. Right: different statistical metrics to analyse the exp. data.

— Regime 2—intermediate Z:
As Z increases, localized instability mechanisms begin to emerge even more, and the buckling behaviour becomes more complex. The worst-case trigger cannot be uniquely assigned to either global or local effects. Instead, both interact in a non-trivial way. In this regime, neither imperfection-sensitivity theory nor local buckling models alone suffice to predict the lower-bound response.
— Regime 3—high Z:

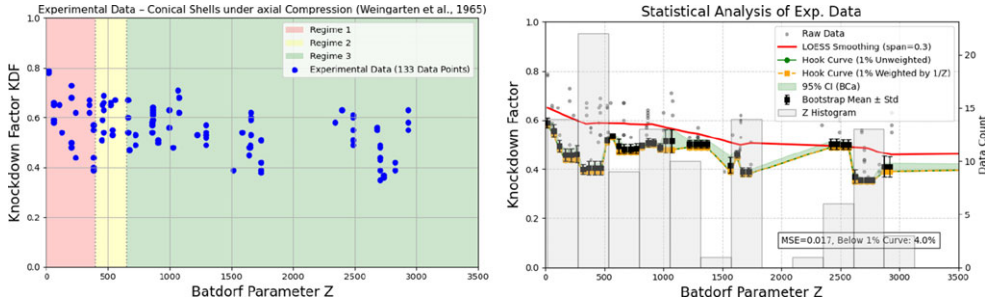

Figure 8. Left: conical shell exp. KDFs from Weingarten *et al*. [9] versus Z, coloured by stability regime. Right: different statistical metrics to analyse the exp. data.

At high slenderness, worst-case-buckling is initiated by localized buckling events—such as snap-through at isolated weak zones—while global imperfections play a subordinate role in worst-case scenarios. Predictive design in this regime requires models that can resolve localized instability, such as the LRSM approach. Though the ultimate collapse may still appear global, its trigger is distinctly local.

Figure 5 (right) shows the evolution of MDC for different manufacturing qualities, quantified by the imperfection amplitude-to-shell thickness ratio w/t. As expected, increasing w/t reduces the overall KDF. More importantly, the boundaries between the three regimes shift with w/t:

— Regime 1 extends to higher Z as w/t increases.
— The onset of Regime 3 is delayed accordingly.

This shows that not only the magnitude of the KDF, but also the dominant buckling trigger, depend on both slenderness and imperfection pattern and severity.

In the theoretical limit of perfect geometry ($w/t = 0$), only localized buckling remains—the shell becomes deterministic, and the KDF is governed solely by intrinsic local instability. This boundary case was first resolved by Wagner *et al*. [33], and it serves as a limiting anchor point for the present probabilistic framework.

(b) Validation with historical data

With the theoretical framework established, we now compare the MDCs with historical experimental data to assess their validity. While this study focuses on cylindrical shells under axial compression, solving this problem inherently provides insights into related stability problems. Conical shells can be approximated as cylindrical models by equating their slant length to the cylinder length and using the average radius of curvature as an approximation for the cylinder radius. This unified approach effectively addresses two major shell stability challenges simultaneously, reinforcing the generality of the MDC framework.

The validation of the MDCs begins with a systematic re-evaluation of historical experimental datasets, spanning from NACA tests in 1933 [34] to NASA campaigns in 1965 [9]. These datasets, covering cylindrical and conical shells under axial compression, were historically analysed using R/t as the primary parameter, which often masked underlying trends in buckling behaviour.

To extract meaningful patterns, we reanalyse these data in terms of the Batdorf parameter Z, which better reflects the stability characteristics of thin-walled shells. Additionally, we incorporate the thickness ratio w/t as a key indicator of manufacturing quality, allowing a more refined classification of test results.

A critical distinction in this analysis is that experimental test series should not be indiscriminately merged into a single dataset. Since w/t inherently reflects fabrication quality,

we assume that within each test campaign, manufacturing conditions were relatively consistent. Consequently, data from different experimental campaigns are analysed separately to avoid conflating variations in fabrication quality with fundamental stability trends.

The goal of this section is to determine whether the MDC can be used to interpret past experimental results in a systematic way. In particular, we seek to identify:

— Whether the historical datasets exhibit consistency with the three regimes (Regimes 1–3) identified by the MDC framework.
— Whether older tests, despite lacking explicit w/t information, exhibit consistent structure when viewed through the lens of MDC.
— Whether past experimental scatter can be better understood, rather than dismissed as purely random variability.

Figures 6–8 present experimental data from three distinct test campaigns on cylindrical and conical shells under axial compression: (figure 6) cylindrical shells tested by Lundquist [34] (NASA), (figure 7) cylindrical shells from Weingarten *et al.* [9] and (figure 8) conical dataset also attributed to Weingarten *et al.* [9]. Despite differences in geometry and likely variations in manufacturing quality (w/t), all three datasets exhibit qualitatively similar structural behaviour when plotted as KDF versus Batdorf parameter Z.

The datasets from Lundquist and the conical shells tested by Weingarten show comparable KDFs in the range $Z \approx 0$ to $Z \approx 3500$, and the corresponding stability regimes align within similar Z intervals. This suggests that the transition from imperfection-dominated to local-buckling-dominated behaviour occurs at consistent slenderness thresholds, regardless of whether the shell is cylindrical or conical. By contrast, the cylindrical shell data from Weingarten display significantly lower minimum KDFs overall—dropping from approximately 0.38 to 0.28 across the Z-range—and the boundaries of the regimes (Regimes 1–3) appear broader and shifted. This observation strongly suggests that the tested shells had poorer manufacturing quality (higher w/t), despite the lack of explicit geometric data.

Importantly, all three datasets qualitatively conform to the characteristic shape of the MDCs. This is not limited to the general trend but includes the detailed structure: a steep initial drop in KDF at low Z, followed by a localized recovery (or 'regeneration') phase, and a renewed decrease towards higher Z. The qualitative agreement between measured data and predicted MDC across different geometries and manufacturing backgrounds provides strong visual support for the proposed regime-based interpretation of shell buckling.

Remarkably, our re-analysis of historical test data through the MDC lens challenges long-held assumptions about early experimental inaccuracies. Where these results were previously dismissed as unreliable due to their perceived scatter, the MDC framework demonstrates they actually cluster precisely where predicted—suggesting the tests were far more accurate than traditionally credited. This revelation rehabilitates decades of experimental work, showing the apparent 'noise' in fact followed the MDC's structured pattern of regime-dependent behaviour.

Beyond qualitative agreement, the MDC is also supported by several independent quantitative metrics, all of which are embedded in figures 6–8 (right). Each metric examines a different aspect of the buckling data—including envelope shape, data distribution, uncertainty and statistical alignment—and consistently supports the structured, non-monotonic form of the 1% quantile curve, summarized in table 1.

Collectively, these quantitative metrics provide compelling statistical evidence that the MDC is not only qualitatively observable but also quantitatively justified. It represents a reproducible feature of shell buckling behaviour across manufacturing variations, geometries and slenderness ratios.

Table 1. Quantitative metrics to analyse MDC shape in exp. data for cylinders under axial compression.

nr.	Metric	description	supports MDC?	comment
1	empirical 1% quantile	lower envelope of experimental KDFs across sliding Z-windows (green curve)	yes	MDC clearly visible (dip—recovery—decline)
2	weighted 1% quantile (1/Z)	corrects for Z-clustering bias (orange dashed curve)	yes	nearly identical to unweighted; confirms robustness
3	LOESS smoothing	non-parametric estimate of conditional mean (red curve)	yes (Weingarten), weak (Lundquist)	MDC visible in Weingarten; masked in Lundquist particularly in transition between Regime 1 and 3
4	bootstrap CI (95% BCa)	confidence band around 1% quantile	yes	MDC persists within CI; not statistical artefact
5	error bars (mean $\pm$ SD)	spread of KDFs within Z-windows	yes	narrow spread supports statistical reliability
6	MSE	mean squared error of fit (0.017–0.032)	yes	low error $\rightarrow$ high alignment with data
7	coverage of 1%-curve	% of data points below the curve (expected: 1%)	yes	actual values: 0–4%; matches statistical expectation

(c) Probabilistic validation

To validate the predictive capability of the MDC, we conducted extensive MC simulations that capture the stochastic nature of thin-shell buckling. These simulations integrate MGIs with localized buckling triggers using the LRSM, providing a comprehensive representation of real-world manufacturing variability and failure mechanisms.

The results confirm a regime-dependent buckling behaviour: at low Batdorf parameters (Regime 1), global imperfection patterns dominate, and shells with larger imperfection amplitudes (high w/t) exhibit the most severe KDFs. As slenderness increases (Regime 3), local buckling triggers govern the weakest specimens, reducing KDFs regardless of w/t magnitude. In between lies Regime 2, the transitional/recovery zone, where competing mechanisms interact and produce a non-monotonic 'regeneration' of the KDF—a hallmark of the MDC.

(i) Key insights from the synthetic data (figure 9):

— The 1% quantile KDF envelope replicates the MDC profile with high fidelity, showing the characteristic dip–recovery–decline structure.
— Manufacturing quality (w/t) systematically shifts regime boundaries while preserving the overall MDC shape.
— Quasi-perfect shells (low $w/t < 0.5$) maintain strong buckling resistance across all Z values—unless failure is triggered by a dominant local buckling event (e.g. a large LRSM patch at a sensitive location).
— The location of local buckling initiation (snap-through) plays a critical role: if the LRSM trigger is placed away from the most sensitive zone (typically mid-height), the global failure mode is less affected, leading to a higher-than-expected KDF despite the presence of a localized instability.

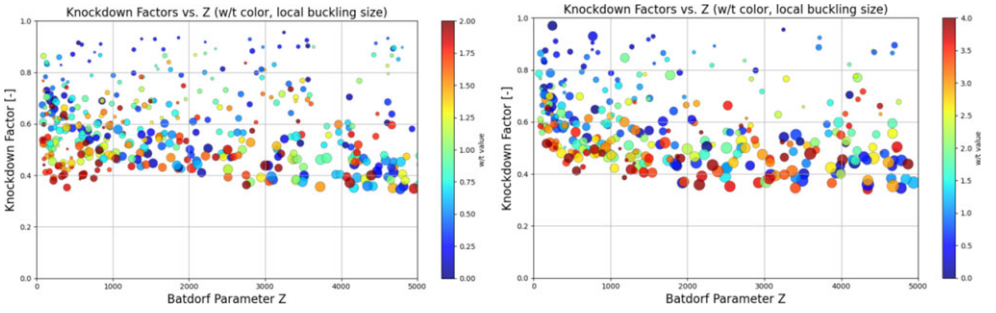

Figure 9. Synthetic KDFs from MC simulations, coloured by w/t and scaled by local buckling relevance. Results for deep-drawing (left) and for axial welding (right).

(ii) Impact of manufacturing process on mechanistic design curve shape

While figure 9 focused on variations in imperfection amplitude (w/t), we also investigated the influence of imperfection morphology induced by different manufacturing processes, deep-drawing (figure 9, left) and axial welding (figure 9, right).

Both datasets exhibit the general regime structure predicted by the MDC. However, the intensity and clarity of the non-monotonic behaviour differ significantly:

— Deep-drawn shells show a pronounced dip and partial recovery around $Z \approx 0$–1000—the canonical 'Hook' shape of the KDF envelope.
— Welded shells, by contrast, display a linear reduction of the KDF envelope with only a subtle recovery around $Z \approx 800$–1000.

This contrast reveals that the MDC shape is process-dependent: its manifestation reflects the spectral character of the underlying imperfection morphology. Specifically, to reach KDFs as low as those observed in deep-drawn shells (with $w/t \approx 2$), welded shells typically require much larger w/t values (≈ 4). This highlights the critical role of both amplitude and spectral content in governing buckling sensitivity.

When comparing the historical experimental data in figure 8 (left) with the purely simulated results in figure 9 (right), one observes a striking similarity in the regime structure for $Z = 0$–1000. The experimental shells were manufactured using axial lap welding, and the simulations in figure 9 (right) likewise reflect axially welded imperfection morphologies. This consistency—despite the simulations being entirely independent—confirms that the MDC shape is not an artefact of fitting, but a physically grounded response to realistic imperfection patterns.

(d) Phenomenological characterization of buckling modes in low-Z shells

MC simulations at $Z = 200$ revealed a striking divergence in failure mechanisms between shells with different imperfection patterns, despite having identical global geometry, manufacturing quality $w/t = 2$ and boundary conditions. Two representative cases were examined, as shown in figure 10: one with a relatively high KDF (KDF = 0.62, axial welded shell ST6 [16]) and another with a significantly lower KDF (0.45, deep drawn shell IW1-33 [35]). Their differences are not merely quantitative—they reflect fundamentally different buckling processes.

The high-KDF shell followed a classical local buckling–triggered buckling: a single imperfection-initiated buckle led to localized instability, resulting in a soft degradation of axial stiffness and an initial drop in load-carrying capacity. In simulation, this manifests as a gradual transition; in practice, such local events often evolve into global buckling through stress redistribution and imperfection interaction. As loading progresses, the localized dimple spreads circumferentially, forming a post-buckling wave pattern with partial load recovery. This response

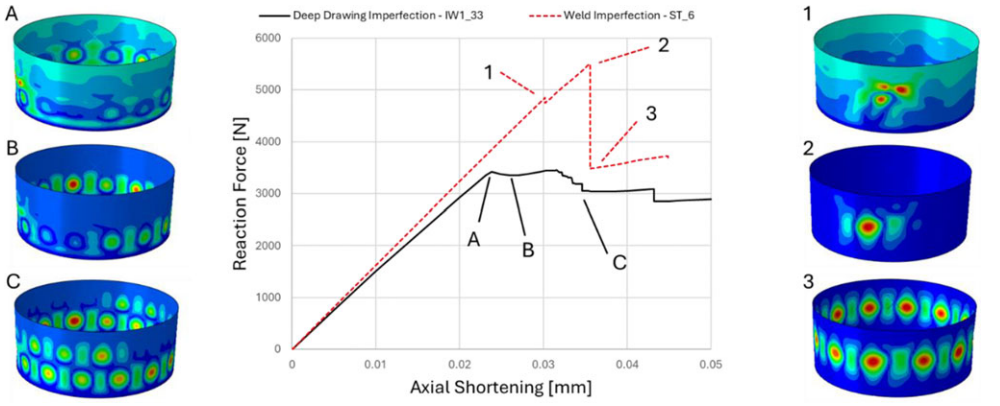

Figure 10. Load–displacement curve for $Z = 200$ shells with different imperfection patterns.

is consistent with slender shells where local buckling is the dominant trigger, but global integrity is not immediately lost—a typical feature of the Local-Trigger Buckling Regime (worst case).

By contrast, the low-KDF shell exhibited a fundamentally different failure mode—the cascade buckling mechanism—characterized by the amplification of global imperfection patterns across the full circumference. Unlike classical local buckling, this progressive collapse resembles the global instability of an axially loaded column: the structure gradually assumes a post-buckling-like shape under increasing load, with the entire circumference participating synchronously before abrupt failure. The force plateaued as multiple buckles formed nearly simultaneously, lacking the clear local-to-global transition seen in conventional buckling.

We propose the term Cascade Buckling to describe this mode, where imperfection patterns trigger a chain reaction of circumferential instability—visually analogous to column buckling but with shell-specific coupling effects. This deceptive progression (structurally stable until sudden collapse) explains why low-Z KDFs are more severe than predicted by local models, revealing a previously overlooked trigger mechanism critical for design safety.

(e) Manufacturing signatures and imperfection morphology

To better understand the variability of shell buckling performance, we analysed a broad set of MGIs from both metallic and composite Carbon Fibre Reinforced Polymer (CFRP) cylindrical shells. These imperfections stem from typical manufacturing processes such as axial welds, machining, electroplating and deep drawing for metal shells, and hand layup or filament winding for CFRP structures. All patterns were mapped to ideal cylindrical geometries and used as inputs in the regime-based MC simulations.

(i) Imperfection signatures from metallic manufacturing processes

A key observation from figure 11 is that the characteristic MDC shape—a non-monotonic dip in KDF at intermediate Batdorf parameters—emerges consistently across all examined metallic manufacturing processes. However, the onset and intensity of this dip differ notably depending on the imperfection morphology associated with each process. Deep-drawn shells exhibit a pronounced minimum already between $Z = 400$ and $Z = 700$, indicating an early transition into the instability-sensitive regime. Electroformed shells follow a similar trend but overall higher KDF values, suggesting that their manufacturing-induced imperfections are less detrimental to structural performance. Machined and axially welded shells lie in between: they also show visible dips around $Z \approx 400$, though with varying depth.

This variation highlights a crucial insight: while the MDC behaviour appears to be a universal feature of imperfection-driven buckling, its specific manifestation is highly sensitive to the

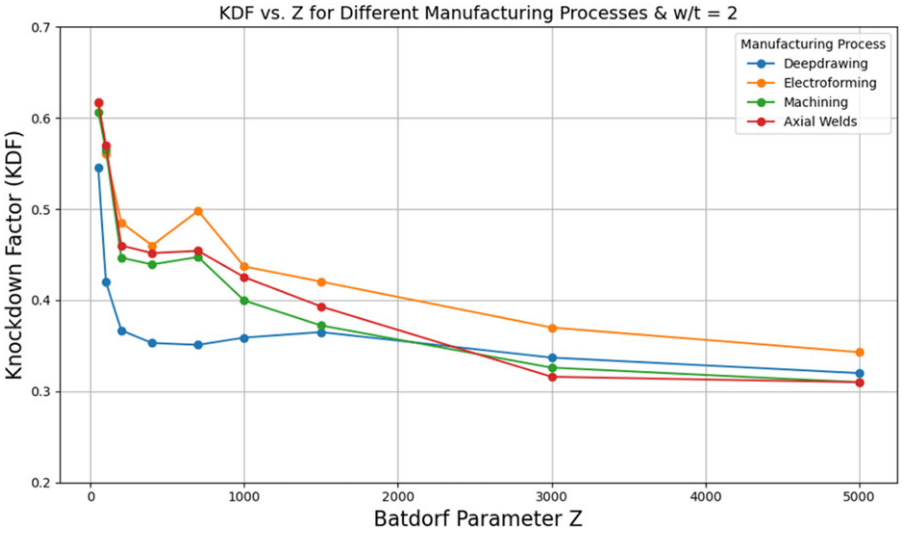

Figure 11. 1% KDF trends for different metallic manufacturing processes for $w/t = 2$.

type and severity of manufacturing-induced imperfections—particularly those introduced by processes commonly used in the fabrication of metallic shells.

Interestingly, the MC simulations reveal that no single imperfection type consistently yields the lowest KDF across all conditions. For instance, while deep drawing generally results in strong knockdown, its relative severity depends on both Z and w/t. In some regimes, imperfections from axial welds or machining may dominate, figure 11. This reinforces the importance of considering the interplay between imperfection morphology, shell geometry and the active stability regime when assessing buckling performance.

Consequently, it is not possible to define a universal worst-case imperfection shape. The most critical configuration depends strongly on geometric parameters and varies across the design space. The MDC framework captures this dependency statistically, but the actual failure-triggering imperfection differs from case to case.

This regime dependency of the worst-case shape makes an MC approach not only justified, but essential: deterministic assumptions (e.g. single-dimple perturbations) cannot capture the shifting failure landscape that emerges with varying Z and w/t.

A spectral comparison of measured imperfections from metallic shells (figure 12) reveals a fundamental difference in morphological character.

The spectral decomposition of MGIs provides a systematic way to characterize typical deformation patterns induced by various manufacturing processes. Based on the extensive evaluation of MC simulations conducted in this study, we find that the most critical imperfection morphologies—i.e. those leading to the lowest KDFs—consistently exhibit a combination of low axial and circumferential wavenumbers. Specifically, high energy concentration in the modes $k = 0$ or 1 (axial wavenumber) and $l = 2$–4 (circumferential wavenumber) is strongly associated with early onset of global-trigger buckling.

This combination produces large-scale global shape deviations, which are particularly effective at destabilizing the shell under axial compression. Our simulations confirm that such patterns frequently result in the lowest KDF outcomes across a wide range of geometric configurations.

The underlying mechanics are intuitive:

— $k = 0$ corresponds to axially symmetric imperfections, deforming the shell uniformly along its length.
— l-values (e.g. $l = 2$–4) produce broad circumferential shapes that do not localize the instability, but instead cause distributed load redirection, triggering premature buckling.

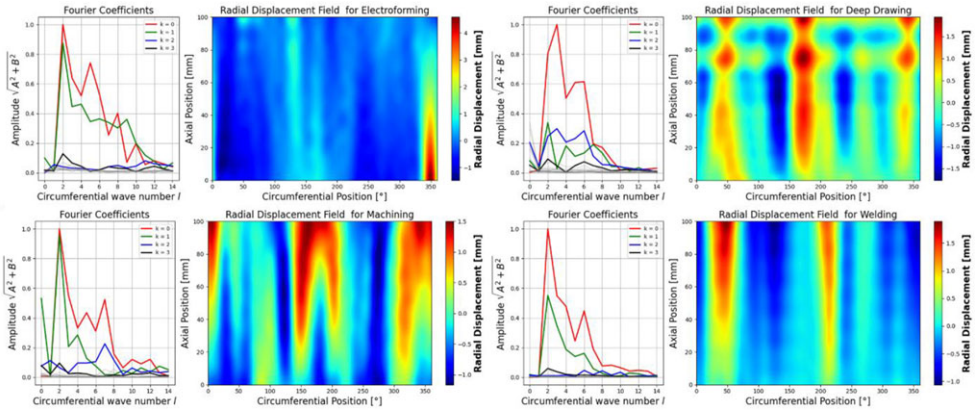

Figure 12. Fourier coefficients and geometric imperfection signatures for the shells according to different metallic manufacturing processes taken from [16] and [35].

These trends are clearly visible in the Fourier spectra of various measured imperfection datasets. For example, deep-drawn shells exhibit precisely this critical spectral signature and show consistently low KDFs in both simulation and historical experimental data. By contrast, processes such as electroforming or filament winding produce more diffuse and less critical distributions, which aligns with their improved buckling performance.

However, it must be emphasized that Fourier-based evaluation alone is not sufficient to predict structural capacity. The actual impact of an imperfection on the buckling load depends on the shell's geometry—particularly the Batdorf parameter Z, slenderness ratio w/t and boundary conditions. Two shells with identical spectral content can exhibit vastly different buckling loads if their geometries differ.

In conclusion, while spectral decomposition provides a powerful means to assess the potential criticality of imperfection patterns, it cannot replace full nonlinear simulation. The findings presented here are grounded in large-scale MC simulations combining measured imperfection data and localized buckling mechanisms, and thus provide a validated, experience-based framework for interpreting and classifying shell imperfection morphologies.

(ii) Imperfection signatures from composite lamination processes

In addition to metallic structures, we also investigated measured imperfection fields from laminated composite shells, specifically CFRP cylinders manufactured via hand layup and filament winding. The Fourier decomposition of these imperfections revealed a distinctly different spectral signature compared with their metallic counterparts. While metallic shells often exhibit significant energy in the critical mode range $k = 0$–1, $l = 2$–4, the composite specimens tend to show less localized energy concentration, with smoother, more distributed patterns and lower overall amplitude in the most dangerous modes.

As illustrated in figure 13, CFRP imperfections exhibit rapidly decaying Fourier spectra dominated by low circumferential mode numbers but with considerably lower energy density. This difference in spectral structure may explain the absence of a pronounced MDC shape in the MC analysis for composites within the examined range of slenderness ratios ($w/t = 0 \ldots 2$). Unlike metallic shells, the expected non-monotonic dip-recovery-decline of the 1% quantile KDF was not observed for composite imperfections in this parameter regime (it forms for $w/t > 3$).

Nonetheless, the lower-bound envelopes derived from our simulations still successfully captured all 222 experimental test cases [31] compiled between 1965 and 2024, as shown in figure 14 (left). This suggests that the MDC framework remains valid for CFRP cylinders, even

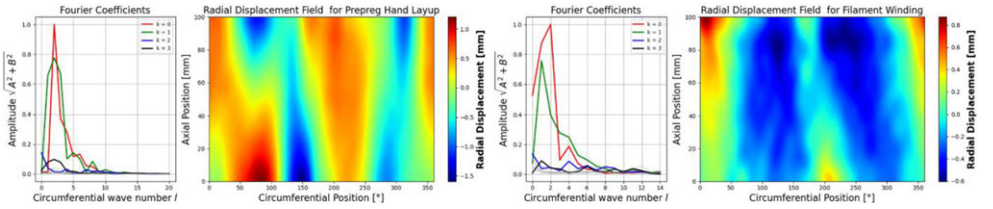

Figure 13. Fourier coefficients and geometric imperfection signatures for the shells according to different composite lamination processes taken from [16] and [36].

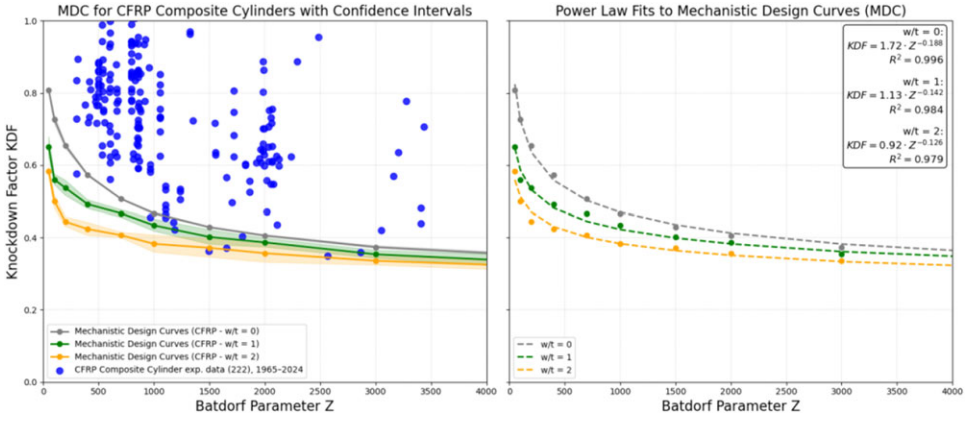

Figure 14. MDC for CFRP: experimental validation based on 222 composite cylinder tests [31] (left) and power law fits (right).

if the spectral mechanisms leading to the characteristic curve shape are not as dominant as in metallic structures.

One possible explanation is that CFRP manufacturing processes inherently suppress the formation of critical global modes, either due to more uniform layup procedures, curing-induced symmetry or the use of mandrels that constrain low-frequency deviations. As a result, many composite imperfections appear less sensitive to global buckling mechanisms, particularly in the lower w/t regime and may instead fail in Regime 2 or Regime 3 mechanisms, depending on Z and w/t.

For practical design use, the MDCs for CFRP composite cylinders were fitted with power laws over a range of $w/t = 0$ to 2, figure 14 (right). These fits enable simple design estimations but are strictly valid only for quasi-isotropic laminates and axially stiff layups (i.e. A11 > A22 in the ABD matrix). Notably, the power law approximation shows reduced accuracy in the low-Z regime ($Z < 400$) for $w/t = 1$–2. In this region, caution is advised and designers should rely on the individual data points rather than the fitted curve.

Further investigations across a broader range of w/t, layup architectures and loading conditions would be required to fully understand the transition behaviour of composite shells. However, the results shown here already suggest that composite-specific design curves may benefit from a separate characterization pathway, while still being bounded conservatively by the same worst-case MDC predictions used for metallic structures.

(f) Summary

This chapter introduces and validates the MDC as a new framework for understanding the stability of axially compressed cylindrical shells. Unlike traditional approaches based on Koiter's

imperfection sensitivity theory—which emphasize asymptotic behaviour near the perfect state—the MDC is built upon mechanistic realism, measured imperfection signatures and statistical robustness derived from thousands of MC simulations.

A central insight of the MDC framework is the regime-dependent nature of shell buckling, characterized by a non-monotonic trend in the 1% quantile KDFs across the Batdorf parameter Z. By capturing this progression, the MDC explains the structured scatter observed in decades of experimental data—a behaviour not predicted by classical imperfection sensitivity theory.

Moreover, the MDC incorporates real-world manufacturing influences by analysing the morphology of MGIs. For metallic shells, the emergence of the MDC's characteristic dip is linked to low-order axial and circumferential Fourier modes (figure 12), while for composites, smoother spectra result in more stable behaviour. In low-Z shells, the MDC identifies the cascade buckling mechanism as a previously overlooked failure mode, where global imperfection patterns lead to abrupt collapse—a process outside the scope of local buckling models.

Equally important, the LRSM, used to model local failure, also follows a mechanistic principle: it does not represent a geometric imperfection *per se*, but directly imposes the structural effect of imperfection-induced membrane collapse. Together, LRSM and MDC establish a unified, mechanism-based paradigm—modelling not imperfection shapes but their structural consequences.

Rather than refining Koiter's theory, the MDC provides a complementary, data-driven alternative that connects physical failure mechanisms with statistically validated predictions. It transforms the interpretation of shell buckling from an abstract sensitivity problem into a mechanism-based, design-oriented discipline, paving the way for regime-aware optimization strategies in engineering practice.

3. Case studies: practical evaluation of the mechanistic design curve framework

While the MDC framework was developed from physical and statistical principles, its practical utility must ultimately be demonstrated through comparison with real-world design cases. The following case studies highlight how the MDC improves the predictive quality of existing design methods and supports mass-efficient, regime-aware structural sizing.

To demonstrate the practical relevance of the MDC approach, we present two representative application cases from the field of aerospace engineering. These examples do not aim to provide a comprehensive evaluation across all possible shell geometries or manufacturing scenarios. Rather, they were deliberately chosen to reflect two realistic and critical use cases in launch vehicle structures: an aluminium cylindrical interstage and a composite conical adapter.

In both cases, we compare the MDC-based design KDFs (from appendix Ad(v)) with traditional values prescribed by NASA guidelines (SP-8007 and SP-8019), highlighting the implications of regime-aware modelling for structural efficiency. An interactive Excel tool implementing the MDC framework is available at https://doi.org/10.5281/zenodo.16636940, allowing engineers to explore the KDF landscape and apply the model to their own design cases.

(a) Aluminium interstage cylinder (Wang *et al*. [14])

The sub-scaled aluminium cylindrical shell ($E = 70\,000$ MPa, $Y = 450$ MPa yield stress) investigated by Wang *et al*. [14] features a radius of 500 mm, a length of 600 mm and a wall thickness of 1.5 mm, resulting in a Batdorf parameter of $Z = 457$. The shell was integrally manufactured using high-precision aerospace fabrication methods, leading to exceptional geometric quality with minimal imperfections—essentially representing a quasi-perfect configuration ($w/t = 0.3$), figure 15.

According to the NASA SP-8007 guideline, such a shell with $R/t = 333$ would be assigned a conservative KDF of KDF = 0.39. However, our MDC framework, which incorporates imperfection morphology and regime-dependent buckling behaviour, yields an estimated 1%

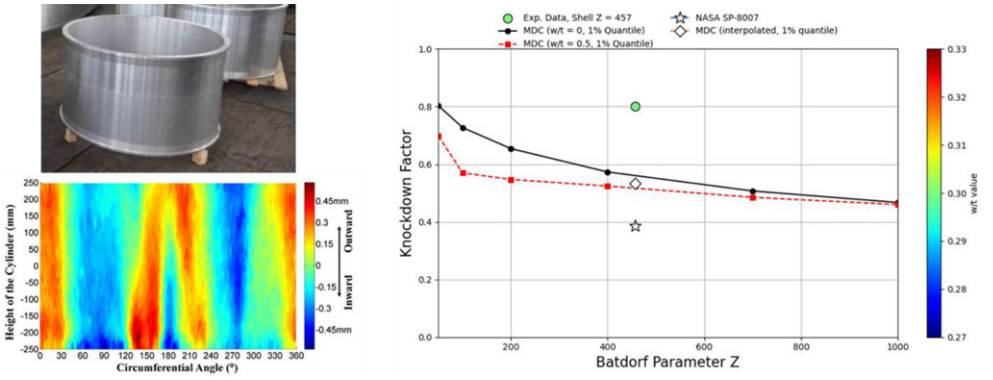

Figure 15. Sub-scaled aluminium cylinder and its imperfection pattern from [14] (left). Comparison of exp. KDFs with NASA SP-8007 and MDC (right).

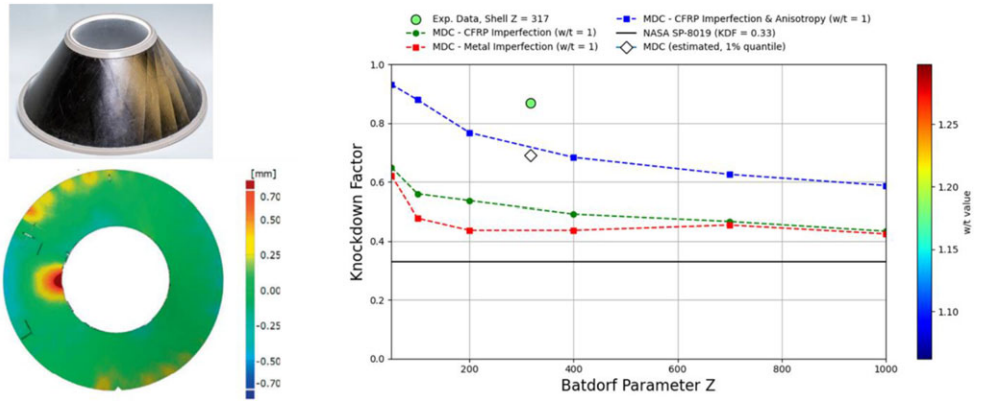

Figure 16. CFRP composite cone and its imperfection pattern from [37] (left). Comparison of exp. KDFs with NASA SP-8019 and different MDC stages (right).

lower-bound KDF of 0.53. This prediction is not only physically justified but also much closer to the actual experimental result of KDF ≈ 0.80.

This comparison underscores the over-conservatism of NASA's legacy design rule in this regime and demonstrates that our regime-aware MDC model offers a safer, yet more efficient prediction—enabling potential mass savings of approximately 14% without compromising structural reliability.

(b) CFRP composite cone (Khakimova *et al*. 2016)

The composite cone K6 studied by Khakimova *et al*. [37] features a semi-vertex angle of 35°, a slant length of 366 mm, a large radius of 400 mm and an effective thickness of 0.75 mm, resulting in a Batdorf parameter $Z = 317$. The cone was manufactured from carbon fibre composite using a [30, 0, −30, −30, 0, 30] layup with high-quality surface accuracy and minimal geometric imperfections, $w/t = 1.18$ [37] (figure 16).

According to traditional NASA guidelines, this structure would be assigned a conservative KDF of KDF = 0.33—NASA SP-8019 (NASA SP-8007, $Rm/t = 480$, KDF ∼ 0.327). By contrast, our MDC methodology enables a three-stage refinement:

1. Metal-specific MDC:
   Yields a 1% quantile KDF of 0.467, already 41% higher than NASA's estimate.
2. Composite-specific MDC:

Raises the KDF to 0.497, improving the prediction by 50%.

3. Anisotropic and composite-specific MDC:
   Further increases the KDF to 0.69, resulting in a 109% improvement over NASA SP-8019.

The predicted value aligns much more closely with the experimental KDF = 0.87, confirming the robustness of this regime-aware methodology. In practical terms, increasing the design KDF from 0.33 to 0.69 allows for up to 31% mass reduction, without compromising safety—a gain of major importance for composite shell structures in lightweight aerospace applications.

While these case studies focus on launch vehicle structures, the underlying methodology is directly applicable to a broader class of shell components, provided that relevant imperfection statistics are available. Future applications may include stiffened shells, domes and hybrid structures under complex loadings.

4. Conclusion and outlook

This study redefines the analysis of shell buckling by revealing the hidden structure behind what has long been regarded as chaotic experimental scatter. Through a large-scale MC framework combining MGIs with localized buckling mechanisms via the LRSM, we introduce the MDC—a regime-based model that captures the systematic transition between global-driven and localization-driven buckling (figure 5). The MDC's key contributions include:

— **Regime-Dependent Buckling**: Replaces the 'one-size-fits-all' imperfection sensitivity approach with three distinct stability regimes (global/transitional recovery/local) that explain previously mysterious experimental scatter.
— **MDC**: Introduces a physics-based predictive framework that captures the non-monotonic 'dip-recovery-decline' pattern of KDFs versus slenderness: a fundamental relationship overlooked for decades.
— **Cascade Buckling Mechanism**: Identifies and names a new failure mode at low slenderness where global imperfections trigger synchronous circumferential collapse, resembling column buckling but with shell-specific coupling effects.
— **Manufacturing-Imperfection Link**: Demonstrates how specific fabrication processes (welding, deep-drawing, etc.) create characteristic imperfection signatures that preferentially trigger certain buckling regimes.
— **Rehabilitation of Historical Data**: Shows that early experimental scatter was not measurement error but structured regime behaviour—forcing re-evaluation of twentieth-century test results.
— **Localized versus Global Trigger Separation**: Resolves the long-standing ambiguity about whether buckling initiates locally or globally by showing both occur but dominate in different slenderness regimes.
— **Regime Shifting as Design Tool**: Proposes actively manipulating shell geometry to 'shift' structures into more favourable buckling regimes (e.g. from local to global) as a deliberate design strategy.

While Koiter's imperfection sensitivity theory provides a foundational understanding of shell buckling, it does not account for the regime-dependent interplay of global and local buckling triggers or the influence of manufacturing signatures. The MDC complements Koiter's framework by offering a data-driven, mechanism-based alternative that reveals structured patterns in experimental data and enables practical design advancements. For example, while dimples [38] are often considered representative imperfections, our results show they only capture worst-case behaviour in high-Z shells (Regime 3). At low Z, global MGI patterns dominate, highlighting the need for regime-specific imperfection models.

The MDC challenges the notion of universal imperfection sensitivity by demonstrating that buckling behaviour is governed by a shifting landscape of failure mechanisms, dependent on

Z and w/t. MC analysis was essential to uncover this structure, as deterministic methods cannot capture the variability of worst-case imperfection shapes. Critics of MC methods, such as Champneys *et al*. [39], raise valid concerns about computational cost and data requirements, but our framework demonstrates that targeted sampling of MGI patterns and LRSM triggers provides robust predictions without exhaustive surveys.

The MDC framework opens new avenues for shell design, reducing reliance on overly conservative guidelines like NASA SP-8007. Future research should extend the MDC to other loading scenarios (e.g. bending, torsion), incorporate nonlinear material behaviour and explore machine learning for automated imperfection classification. Ultimately, this work establishes a foundation for a fully data-driven, regime-aware design methodology that captures the richness of thin-walled instability with physical realism and statistical robustness.

Data accessibility. All datasets used in this study are openly available via Zenodo: ESM Tool Reference [40] and Combined Supplementary Dataset [41]. All supporting materials used in this study are openly available via Zenodo. These include the Excel-based MDC Buckling Tool for calculating regime-aware KDFs, as well as datasets of MGIs, MC-based KDF tables and Python Scripts for Figure-Generation. These resources enable full traceability of the MDC framework and support its use in both academic research and engineering design.

The data are provided in the electronic supplementary material [42].

Declaration of AI use. We have used AI-assisted technologies in creating this article.

Authors' contributions. H.N.R.W.: conceptualization, data curation, formal analysis, methodology, project administration, validation, visualization and writing—original draft; C.H.: formal analysis, funding acquisition, investigation, resources, writing—original draft and writing—review and editing; R.K.: resources, writing—original draft and writing—review and editing; S.N.: writing—review and editing; M.W.: data curation, validation and visualization; and J.Z.: funding acquisition, resources, supervision, validation.

All authors gave final approval for publication and agreed to be held accountable for the work performed therein.

Conflict of interest declaration. We declare we have no competing interests.

Funding. We received no funding for this study.

Acknowledgements. The authors would like to express their sincere gratitude to Prof. Ulrich Römer for his valuable guidance in probabilistic analysis and to Prof. Isaac Elishakoff for his insightful editorial support and his pioneering contributions to probabilistic methods. His paper 'Probabilistic resolution of the twentieth-century conundrum in elastic stability' was a key source of inspiration and helped fuel the persistence needed to complete this work.

Special thanks go to Adam Sadowski and Alexander Evkin for their thoughtful and constructive reviews, which significantly improved the clarity of the manuscript.

The authors also acknowledge the foundational work of Prof. Johann Arbocz, whose Delft imperfection data bank, created in 1979, played a pivotal role in this study. Though long overlooked, this dataset proved instrumental in uncovering the mechanisms described herein.

This work reflects the outcome of seven years of research. The core concept—the characteristic MDC (formerly referred to as the 'Hook Curve')—was initially observed by the first author in 2018 in the dataset shown in figure 8 but could not be fully explained at the time. The peculiar trend—where the KDF first decreases, then increases and eventually decreases again—seemed illogical and could only be interpreted within the limits of the understanding available at the time. The first author tentatively referred to this as 'short shell behaviour', which, in retrospect, was not far from today's concept of low-Z sensitivity. In hindsight, such discomfort—when data defies intuition—often signals the presence of a deeper mechanism waiting to be discovered. The persistent effort to understand and validate this phenomenon ultimately led to the results presented in this paper.

Technical appendix A

(a) Finite element model

For the MC simulations, the cylindrical shells were discretized using linear shell elements (ANSYS SHELL181). The element length was selected according to the guideline $0.5\sqrt{Rt}$, following the recommendation in [12]. Both cylinder ends were modelled with clamped boundary conditions, implemented via remote displacement constraints tied to reference points to enforce rigid-body

behaviour at the edges. To apply the axial compression, the upper edge was allowed to move freely along the axial direction. Nonlinear buckling analyses were performed using the Static Structural solver in ANSYS, with large deformation effects enabled to capture post-buckling behaviour accurately.

(b) Geometric imperfection

(i) Terminology clarification: imperfections versus instabilities

To ensure clarity and consistency with the shell buckling literature, we distinguish between commonly conflated concepts:

> **Geometric Imperfections**: Any deviation from the ideal shell shape, including measured global imperfection patterns (MGIs) (e.g. from manufacturing processes like welding or deep drawing) and local imperfections (e.g. dimples or cutouts). MGIs are characterized by their spatial distribution and amplitude-to-thickness ratio w/t, with critical patterns often exhibiting low axial $k = 0$–1 and circumferential $l = 2$–4 wavenumbers (§2e, figure 12).
> **Local Buckling**: An instability mechanism triggered by localized geometric or material weaknesses, modelled deterministically using the LRSM (see appendix Ac). Local buckling does not refer to an imperfection shape but to the failure process, which can be initiated by various triggers, including dimples, stress concentrations, cutouts or global MGI patterns.
> **Global Buckling**: A failure mechanism driven by large-scale imperfection patterns, often leading to abrupt, multi-buckle collapses, such as the cascade buckling mode at low Z (§2d). Global buckling is distinct from local buckling in its trigger mechanism and deformation pattern.
> **Dimple-type Imperfections**: Canonical local imperfections used in literature as worst-case shapes [38]. However, they only represent a subset of possible deviations and are less critical at low Z, where global MGIs dominate (§2a).
> **Trigger versus Mechanism**: Trigger: initiates failure (dimple, cutout); mechanism: how failure unfolds (snap-through, local buckling).

This distinction is crucial: imperfections define the initial geometry, while buckling mechanisms govern the failure process. The MDC captures the regime-dependent interplay between these mechanisms, showing how global imperfections dominate at low Z (Regime 1), local buckling prevails at high Z (Regime 3) and a complex interaction occurs in the transitional Regime 2 (§2a, figure 5). By clarifying these terms, we align with Koiter's imperfection sensitivity framework while highlighting the MDC's novel contribution: a regime-based classification that extends beyond universal imperfection sensitivity to address real-world manufacturing and design challenges.

(ii) Fourier representation of real measured geometric imperfections

The data used in this section originate from a comprehensive experimental campaign conducted at TU Delft, which forms the basis of the imperfection data repository detailed in [43,44]. The focus here lies on the mathematical characterization of the MGIs using a Fourier-based representation. Readers seeking additional information on the test set-up and evaluation procedures are referred to [45] and to the documentation provided by Dancy [36].

The geometric imperfection fields of the metallic shell specimens were recorded experimentally and decomposed into Fourier coefficients A_{kl} and B_{kl} using the half-wave cosine expansion method, as described in [16].

The half-wave cosine method described in [17] is expressed in equation (A 1) and provides a parametric representation of the imperfection field $z(x,y)$ over the cylindrical shell surface.

This approximation depends on the shell geometry—specifically the length L, radius R and wall thickness t—as well as on the spatial coordinates x and y and the corresponding axial and circumferential wavenumbers k and l. The summation limits n_1 and n_2 define the maximum number of axial and circumferential modes included in the series expansion.

$$z(x,y) = t\sum_{k=0}^{n_1}\sum_{l=0}^{n_2}\cos\left(k\pi\frac{x}{L}\right)\cdot\left(A_{kl}\cos\left(\frac{ly}{R}\right)+B_{kl}\sin\left(\frac{ly}{R}\right)\right). \tag{A 1}$$

(c) Localized reduced stiffness method for local buckling

The LRSM is built upon the characteristic membrane stress state observed in axially compressed cylindrical shells. When pronounced localized imperfections are present, they can initiate local buckling, which in turn may evolve into global instability—a phenomenon often referred to as snap-through buckling (figure 17, left). This instability mechanism leads to a near-complete release of membrane stresses in the affected zone, effectively reducing them to zero along the axial path of the imperfection (figure 17, right).

Such behaviour is closely associated with the characteristic lower-bound plateau of the critical buckling load, commonly observed in thin-walled shells. Once this stress collapse has occurred, further increases in imperfection amplitude in that region no longer affect the buckling load, as the membrane force contribution has already vanished [30].

The LRSM is not introduced as a local imperfection in the classical sense, but rather as a mechanistic surrogate for the failure process induced by imperfections. The core idea is that imperfections, such as dimples, lead to a local collapse of membrane stresses—the main load-carrying mechanism in shells. Instead of introducing a specific imperfection shape (e.g. dimple), we directly impose the resulting effect—the local loss of membrane stiffness—to replicate the critical instability. In this sense, the LRSM models the failure trigger, not the initial imperfection geometry. This distinguishes the approach from Koiter's framework, which links geometric deviations to energy reductions, but does not explicitly model regime-dependent stiffness collapse.

In the LRSM framework, membrane stiffness is selectively reduced within a confined region of the shell to replicate the limiting membrane stress state associated with local buckling.

While the LRSM introduces a localized instability artificially this step is not arbitrary. In practice, local buckling can be triggered by various imperfection types—including unresolved geometric features due to limited MGI resolution [46], thickness variations, material inhomogeneities or load imperfections such as uneven shell edges. However, such data are often incomplete, difficult to obtain or prohibitively expensive to measure—particularly for thin-walled structures manufactured at scale. Rather than attempting to capture all possible imperfection sources explicitly, we use the LRSM to deliberately trigger local buckling in a controlled and repeatable manner. This approach ensures that the structure's sensitivity to localized instabilities is systematically explored—even when the exact trigger remains unknown or unmeasured. The goal is not to reproduce every possible imperfection scenario, but to statistically quantify their potential impact on structural capacity.

A schematic depiction of the area selected for membrane stiffness reduction in the cylindrical shell is presented in figure 18 (left). The cylindrical shell consists of two distinct regions: the main shell surface and a reduced membrane stiffness surface. The main shell surface is modelled in ANSYS using a standard shell section, defined either by a homogeneous thickness or a composite layup. By contrast, the reduced stiffness region is defined via the ABD matrix approach, where all nine components of the membrane stiffness matrix A are divided by a reduction factor α [30], while the bending-extension coupling matrix B is set to zero. For all studies, the membrane stiffness reduction factor was set to $\alpha = 1000$, which represents a converged value ($\alpha > 1000$ do not further reduce buckling load for cylinder under axial compression) based on prior sensitivity analyses [30].

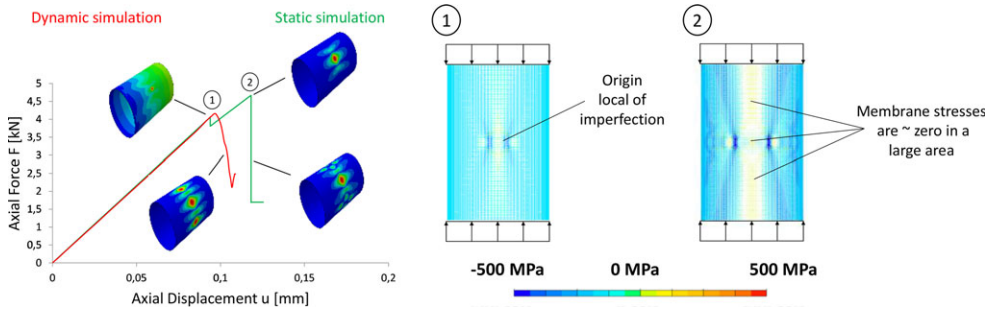

Figure 17. Load–displacement curve for local buckling (left), membrane stress state of a cylinder (right) from [32].

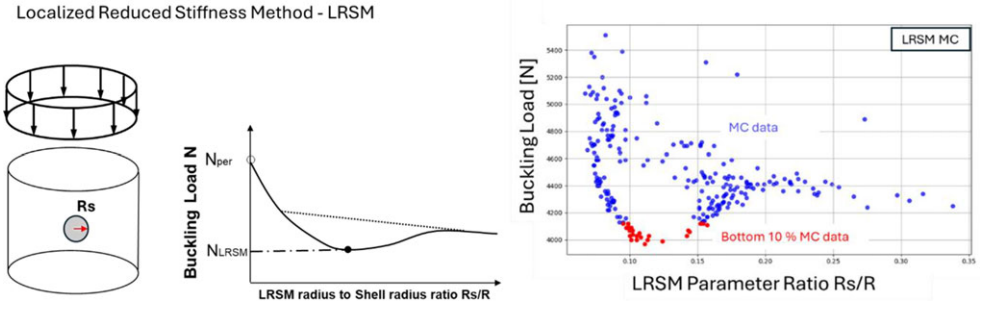

Figure 18. LRSM theory [30] (left) and implementation within MC framework (right).

When applying the LRSM to composite shells, all components of the bending-extension coupling matrix B must be set to zero within the locally reduced stiffness region. This step is necessary to avoid numerical singularities in the global stiffness matrix.

To systematically assess the sensitivity of the buckling load to the extent of the weakened zone, the radius of the LRSM region Rs is varied relative to the shell radius R. By incrementally increasing the size of this region, the influence of localized stiffness loss on the global buckling behaviour can be quantified. The resulting minimum buckling load obtained from this parameter study—illustrated in the LRSM characteristic diagram (figure 18—left)—is then taken as the design-relevant lower bound.

(d) Monte Carlo analysis for determining the 1% quantile of the buckling load

The nonlinear stability of cylindrical shells subjected to axial compression remains a critical challenge due to their extreme sensitivity to imperfections. Traditional deterministic approaches fail to capture the stochastic nature of buckling loads, necessitating a robust numerical strategy. To systematically determine the 1% quantile of the buckling load, an MC-based approach similar to [47,48] was employed, incorporating MGIs and localized buckling effects.

(i) Methodology: geometrically nonlinear analysis with randomized imperfections

Each MC realization involves a geometrically nonlinear analysis with imperfections (GNIA) after [49], where four key parameters are randomly varied:

1. Selection of a MGI Pattern
   - A dataset of about 70 experimentally MGI fields is available, ensuring realistic initial geometry deviations.

— The imperfections are normalized to the shell thickness ($w/t = 1$), meaning the maximum deviation of the chosen pattern is normalized to the shell thickness, independent of its shape.
— This approach allows for an unbiased evaluation of the effect of imperfection geometry without absolute scaling factors affecting the results.

2. Definition of Local Buckling Position
   — A localized buckling trigger is randomly positioned on the cylindrical shell surface.
   — While only one LRSM patch is applied per realization, this simplification is justified by experimental evidence: most failures are initiated by a single dominant buckle. Moreover, adding multiple LRSM sites would increase computational cost and complexity without significantly improving predictive fidelity, as multi-defect effects are already implicitly captured by the measured MGI fields.
   — The location is defined by two randomly sampled parameters:
     (i) axial coordinate z (uniformly distributed along the shell height), and
     (ii) circumferential position θ (uniformly distributed around the shell circumference).
3. Definition of Local Buckling Amplitude
   — The amplitude (patch size) of the local buckling trigger is also randomly chosen.
   — The values are drawn from a uniform distribution but restricted to the range (bottom 10%) leading to the lowest possible buckling load within the LRSM, as shown in (figure 18—right).
   — This ensures that only physically relevant localized imperfections affecting critical load reductions are considered.
4. Execution of the GNIA-Simulation
   — The randomly selected imperfections are incorporated into a fully nonlinear finite element simulation.
   — The force–displacement curve is recorded, and the maximum load is extracted.
   — Each simulation result is stored in a dataset for statistical evaluation.
   — A total of 250 independent realizations are conducted for each cylindrical geometry Z.

(ii) Convergence analysis of the Monte Carlo simulations

Since the primary objective is to determine the 1% quantile of the buckling load, ensuring numerical convergence is essential. Multiple convergence criteria are applied to validate the statistical stability of the MC results:

1. Relative Change in the 1% Quantile
   — The difference between the last two computed 1% quantiles is monitored.
   — If the relative change falls below a predefined threshold, the simulation is deemed converged.
2. Bootstrap Error Band Analysis
   — A bootstrapping method (resampling with replacement) is applied to estimate the standard deviation of the 1% quantile.
   — If the bootstrapped confidence interval is sufficiently narrow, the result is considered stable.
3. Wasserstein Distance Metric
   — The Wasserstein distance is computed between successive subsets of the MC dataset to quantify changes in the probability distribution.
   — If the Wasserstein distance falls below a threshold, the distribution is assumed to have stabilized.

4. Kolmogorov–Smirnov (KS) Test
    - The KS test is performed between consecutive subsets of the MC dataset to assess whether they originate from the same distribution.
    - A high p-value indicates that the dataset has reached statistical stability.

By combining these four independent convergence criteria, a robust statistical estimate of the 1% quantile is obtained, ensuring computational efficiency without excessive simulations. Based on these criteria, 250 realizations per Z-value were determined to be sufficient for convergence.

(iii) Monte Carlo simulation results

The MC analysis for each cylindrical shell geometry Z provides the 1% quantile of the buckling load along with its 99% confidence interval (upper and lower bounds). To construct a complete MDC for a given imperfection-to-thickness ratio ($w/t = 1$), simulations were performed at the following Batdorf parameter values:

$$Z = 50, 100, 200, 400, 700, 1000, 1500, 2000, 3000, 5000, 10\,000$$

For each of these values, 250 independent GNIA simulations were conducted, resulting in a total of 2750 simulations per MDC. To assess the influence of the imperfection-to-thickness ratio on the buckling response, the entire process was repeated for w/t values ranging from 0 to 8.

This extensive numerical investigation provided not only a statistically robust estimate of the buckling load but also key physical insights into the effects of imperfection placement and shape on shell stability.

(iv) Implications and conclusion

The MC-based GNIA framework introduced in this study enables a mechanistic and statistically robust prediction of shell buckling behaviour under realistic imperfections. By combining measured geometric data (MGIs), localized failure triggers (via the LRSM) and nonlinear simulations, we construct MDCs that reveal a structured, regime-dependent stability landscape.

Key implications include:

- A clear differentiation between Regime 1 (global imperfection–triggered collapse) and Regime 3 (local instability via membrane collapse), with a transitional Regime 2 in between.
- A departure from classical shape-based imperfection modelling: both MDC and LRSM represent mechanistic effects, not geometric deviations.
- Predictive lower bounds for KDFs across varying Z and w/t, enabling weight-optimized, fabrication-aware design.
- A reinterpretation of historical test scatter as structured behaviour, rather than randomness—replacing empirical KDFs with physics-based quantiles.

Importantly, only in the theoretical limit of perfect geometry ($w/t = 0$) does a single failure mechanism dominate. In all practical cases, the buckling response is regime-specific and must be modelled accordingly.

This study reframes shell buckling as a mechanistically driven, data-informed design problem, laying the foundation for future research and improved design standards.

(v) MDC for metallic cylinders with application boundaries

The MDC KDFs presented here are derived from extensive MC simulations, following a consistent set of modelling assumptions to ensure robustness and comparability. The primary constraints include figure 19:

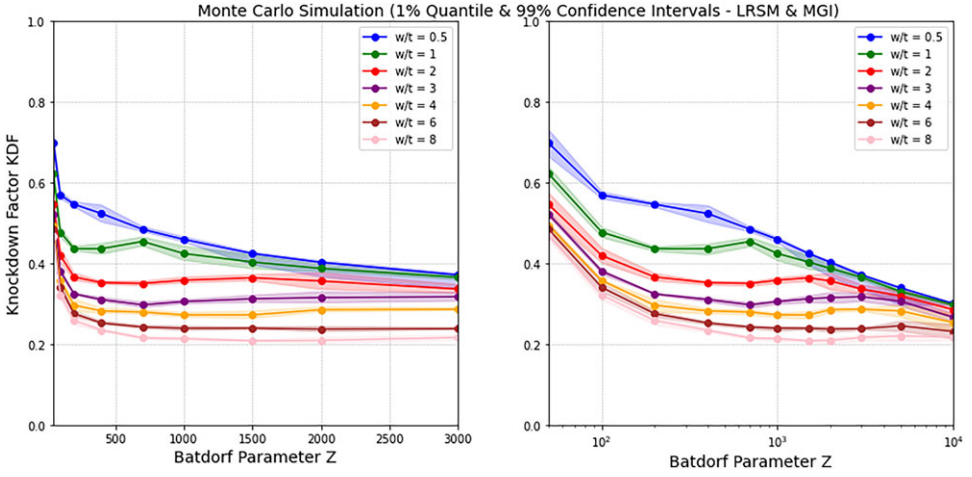

Figure 19. MDC with 99% confidence intervals: linear scale (left), log scale (right).

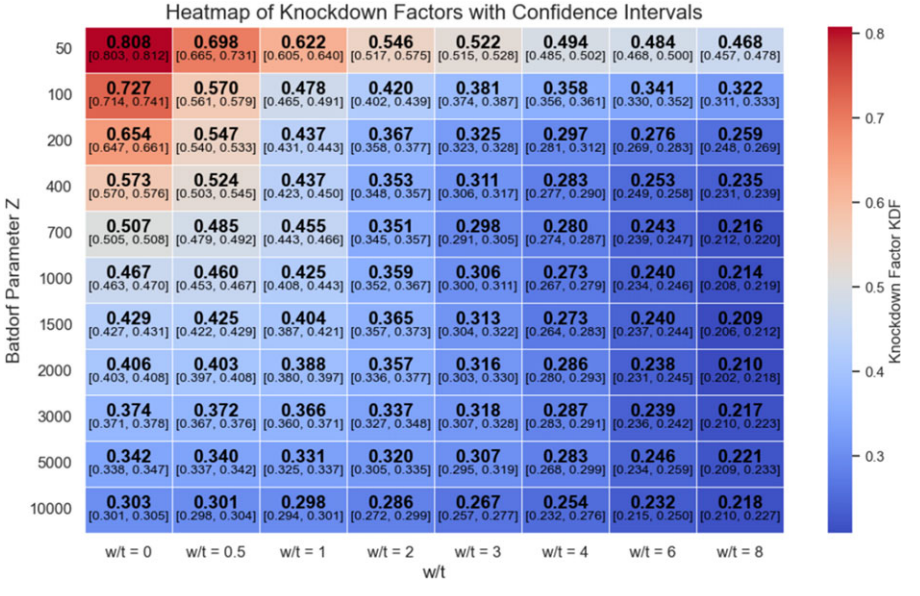

Figure 20. Heatmap of the MDC data: KDF of 1% quantile with 99% confidence intervals.

— Boundary conditions: The shell is clamped at both, while one end remains free to move axially, allowing compression to be applied.
— Material properties: The analysis assumes an isotropic, homogeneous material.
— Linearity assumption: The study considers linear-elastic stability for relative slenderness ratios $\lambda > 1.45$ with $\lambda = \sqrt{\text{yield stress/elastic buckling stress}} = \sqrt{Y/\sigma_{\text{theory}}}$.
— Imperfection types: The MC dataset accounts for typical metal shells (machining, axial welding, electroplating and deep drawing) but does not account for strong radial imperfections (e.g. welded joints, circumferential misalignments), meaning the MDC may not be valid for shells with dominant manufacturing defects in this category.

The MDC KDFs for metal shells are given in figure 20 as a heatmap.

References

1. Hutchinson J, Thompson J. 2018 Imperfections and energy barriers in shell buckling. *Int. J. Solids Struct.* **148–149**. 157–168. (doi:10.1016/j.ijsolstr.2018.01.030)
2. Teng J, Rotter J. 2003 *Buckling of thin metal structures*. London, UK: CRC Press.
3. ECCS. 2008 *Buckling of steel shells: European design recommendations*, 5th edn. Brussels, Belgium: European Convention for Constructional Steelwork.
4. von Karman T, Dunn L, Tsien H. 1940 The influence of curvature on the buckling characteristics of structures. *Journal of the Aeronautical Sciences* **7**, 276–289. (doi:10.2514/8.1123)
5. Koiter WT. 1945 The stability of elastic equilibrium. PhD thesis, Delft University of Technology, The Netherlands.
6. Hühne C, Rolfes R, Breitbach E, Teßmer J. 2008 Robust design of composite cylindrical shells under axial compression — Simulation and validation. *Thin-Walled Structures* **46**, 947–962. (doi:10.1016/j.tws.2008.01.043)
7. Peterson JP, Seide P, Weingarten VI. 1968 Buckling of thin-walled circular cylinders—NASA SP-8007. Technical Report.
8. Weingarten V, Seide P. 1968 NASA SP-8019—buckling of thin-walled truncated. NASA Space Vehicle Design Criteria.
9. Weingarten VI, Morgan EJ, Seide P. 1965 Elastic stability of thin-walled cylindrical and conical shells under axial compression. *AIAA Journal* **3**, 500–505. (doi:10.2514/3.2893)
10. Elishakoff I. 1983 How to introduce the imperfection sensitivity concept into design. In *Collapse: buckling of structures in theory and practice*), pp. 345–357. Cambridge, UK: Cambridge University Press.
11. Fina M, Weber P, Wagner W. 2020 Polymorphic uncertainty modeling for the simulation of geometric imperfections in probabilistic design of cylindrical shells. *Structural Safety* **82**, 101894. (doi:10.1016/j.strusafe.2019.101894)
12. Wullschleger L, Meyer-Piening HR. 2002 Buckling of geometrically imperfect cylindrical shells - definition of a buckling load. *Int. J. Non-Linear Mech.* **37**, 645–657. (doi:10.1016/S0020-7462(01)00089-0)
13. Hilburger MW. 2018 On the Development of Shell Buckling Knockdown Factors for Stiffened Metallic Launch Vehicle Cylinders. In *2018 AIAA/ASCE/AHS/ASC Structures, Structural Dynamics, and Materials Conference, AIAA SciTech Forum, Kissimmee, FL*.
14. Wang B, Zhu S, Hao P, Bi X, Du K, Chen B, Ma X, Chao Y. 2018 Buckling of quasi-perfect cylindrical shell under axial compression: a combined experimental and numerical investigation. *Int. J. Solids Struct.* **130–131**, 232–247. (doi:10.1016/j.ijsolstr.2017.09.029)
15. Schillo C, Röstermundt D, Krause D. 2015 Experimental and numerical study on the influence of imperfections on the buckling load of unstiffened CFRP shells. *Compos. Struct.* **131**, 128–138. (doi:10.1016/j.compstruct.2015.04.032)
16. Arbocz J, Abramovich H. 1979 *The initial imperfection data bank at the Delft University of Technology, Part 1*. Department of Aerospace Engineering, Report LR-290. Delft, The Netherlands: Delft University of Technology.
17. Kriegesmann B, Rolfes R, Hühne C, Teßmer J, Arbocz J. 2010 Probabilistic design of axially compressed composite cylinders with geometric and loading imperfections. *Int. J. Struct. Stab. Dyn.* **10**, 623–644. (doi:10.1142/S0219455410003658)
18. Takano A. 2012 Statistical knockdown factors of buckling anisotropic cylinder under axial compression. *J. Appl. Mech.* **79**, 051004. (doi:10.1115/1.4006450)
19. Franzoni F. 2020 Predicting buckling from vibration: an analytical, numerical, and experimental verification for cylindrical shells. Dissertation, Universität Bremen, Germany.
20. Degenhardt R, Bethge A, Kling A, Zimmermann R, Rohwer K. 2007 *Probabilistic approach for improved buckling knock-down factors of CFRP cylindrical shells*. In Proceeding of 18th Engineering Mechanics Division Conference.
21. Khakimova R, Castro S, Wilckens DRK, Degenhardt R. 2017 Buckling of axially compressed CFRP cylinders with and without additional lateral load: Experimental and numerical investigation. *Thin-Walled Structures* **119**, 178–189. (doi:10.1016/j.tws.2017.06.002)
22. Tian K, Wang B, Hao P, Waas A. 2017 A high-fidelity approximate model for determining lower-bound buckling loads for stiffened shells. *Int. J. Solids Struct.* **148–149**, 14–23. (doi:10.1016/j.ijsolstr.2017.10.034)

23. Starnes JHJ, Hilburger MW, Nemeth MP. 2000 The Effects of Initial Imperfections on the Buckling of. In *Composite structures - theory and practice* (eds P Grant, CQ Rousseau), pp. 529–550. ASTM STP 1383. West Conshohocken, PA: ASTM International.
24. Schultz MR, Sleight DW, Myers DE, Waters WA, Chunchu PB, Lovejoy AW, Hilburger MW. 2016 Buckling Design and Imperfection Sensitivity of Sandwich Composite Launch-Vehicle Shell Structures. In *Proc. American Society for Composites: 31st Tech. Conf., Williamsburg, VA*.
25. Wang B, Du K, Peng H, Tian K, Chai Y, Jiang L, Xu S, Zhang X. 2019 Experimental validation of cylindrical shells under axial compression for improved knockdown factors. *Int. J. Solids Struct.* **164**, 37–51. (doi:10.1016/j.ijsolstr.2019.01.001)
26. Bazant Z, Cedolin L. 2010 *Stability of structures: elastic, inelastic, fracture and damage theories*. Singapore: World Scientific.
27. Evkin A. 2018 Local buckling of cylindrical shells - Pogorevlov's geometrical method. In *Special issue: problems of nonlinear mechanics and physics of materials*. Berlin, Germany: Springer-Verlag.
28. Groh R, Pirrera A. 2019 On the role of localizations in buckling of axially compressed cylinders. *Proc. R. Soc. A* **475**, 20190006. (doi:10.1098/rspa.2019.0006)
29. Castro SG, Zimmermann R, Arbelo MA, Khakimova R, Hilburger MW, Degenhardt R. 2014 Geometric imperfections and lower-bound methods used to calculate knock-down factors for axially compressed composite cylindrical shells. *Thin-Walled Structures* **74**, 118–132. (doi:10.1016/j.tws.2013.08.011)
30. Wagner H, Sosa E, Hühne C, Ludwig T, Croll J. 2019 Robust design of imperfection sensitive thin-walled shells under axial compression, bending or external pressure. *Int. J. Mech. Sci.* **156**, 205–220. (doi:10.1016/j.ijmecsci.2019.02.047)
31. Hartwich TS, Panek S. 2023 Database of Static Buckling Experiments with Cylindrical Composite Shells under Axial Compression [Data set]. Zenodo. (doi:10.5281/zenodo.7843039)
32. Wagner H. 2018 Robust Design of Buckling Critical Thin-Walled Shell Structures. PhD thesis, Technical University Carolo-Wilhelmina, DLR Forschungsbericht 2019-14, Germany.
33. Wagner HN, Hühne C, Niemann S, Khakimova R. 2017 Robust design criterion for axially loaded cylindrical shells - simulation and validation. *Thin-Walled Structures* **115**, 154–162. (doi:10.1016/j.tws.2016.12.017)
34. Lundquist EE. 1934 *Strength test of thin-walled duralumin cylinders in compression*. Langley Field, VA: Langley Aeronautical Laboratory, National Advisory Committee for Aeronautics (NACA).
35. Dancy R, Jacobs D. 1988 *The initial imperfection data bank at the Delft University of Technology: Part II*. Report LR-559. Delft, The Netherlands: Faculty of Aerospace Engineering, Delft University of Technology. Available at: https://resolver.tudelft.nl/uuid:9da23db8-dba9-4464-96cf-e733ee924019.
36. Schillo C, Kriegesmann B, Krause D. 2017 Reliability based calibration of safety factors for unstiffened cylindrical composite shells. *Compos. Struct.* **168**, 798–812. (doi:10.1016/j.compstruct.2017.02.082)
37. Khakimova R, Wilckens D, Reichardt J, Degenhardt R. 2016 Buckling of axially compressed CFRP truncated cones: Experimental and numerical investigation. *Compos. Struct.* **146**, 232–247. (doi:10.1016/j.compstruct.2016.02.023)
38. Horak J, Lord JG, Peletier M. 2006 Cylinder buckling: the mountain pass as an organizing center. *SIAM J. Appl. Math.* **66**, 1793–1824. (doi:10.1137/050635778)
39. Champneys AR, Dodwell TJ, Groh RM, Hunt GW, Neville RM, Pirrera A, Sakhaei AH, Schenk M, Wadee MA. 2019 Happy catastrophe: recent progress in analysis and exploitation of elastic instability. *Front. Appl. Math. Stat.* **5**, 34. (doi:10.3389/fams.2019.00034)
40. Wagner H. 2025 MDC Buckling Tool v1.2.07 – Excel implementation for probabilistic shell buckling analysis [Data set]. Zenodo. (doi:10.5281/zenodo.16636940)
41. Wagner H. 2025 Supplementary data for 'Structured Chaos': Python scripts, Monte Carlo results, and imperfection data [Data set]. Zenodo. (doi:10.5281/zenodo.16636929)
42. Wagner HNR, Hühne C, Khakimova R, Niemann S, Wang M, Zhang J. 2025 Structured chaos: redefining the design of buckling-critical cylindrical shells. Figshare. (doi:10.6084/m9.figshare.c.7987106)
43. Arbocz J. 1982 The imperfections data bank, a means to obtain realistic buckling loads. In *Buckling of shells* (ed. E Ramm).
44. Verduyn W, Elishakoff I. 1982 *A testing machine for statistical analysis of small imperfect shells: part 1*. Delft, Netherlands: Delft University of Technology, Department of Aerospace Engineering.

45. de Vries J. 2005 *Research on the Yoshimura buckling pattern of small cylindrical thin walled shells*. In Noordwijk, The Netherlands: Proceedings of the European Conference on Spacecraft Structures, Materials and Mechanical Testing.
46. Kepple J, Herath M, Pearce G, Prusty B, Thomson R, Degenhard R. 2015 Stochastic analysis of imperfections sensitive unstiffened composite cylinder using realistic imperfections models. *Compos. Struct.* **126**, 159–173. (doi:10.1016/j.compstruct.2015.02.063)
47. Elishakoff I. 2012 Probabilistic resolution of the twentieth century conundrum in elastic stability. *Thin-Walled Structures* **59**, 35–57. (doi:10.1016/j.tws.2012.04.002)
48. Elishakoff I, Arbocz J. 1985 Reliability of axially compressed cylindrical shells with general nonsymmetric imperfections. *ASM International* **52**, 122–128.
49. Sadowski A *et al.* 2023 8-MW wind turbine tower computational shell buckling benchmark. Part 1: An international 'round-robin' exercise. *Eng. Fail. Anal.* **148**, 107133. (doi:10.1016/j.engfailanal.2023.107133)

Glossary

L	Cylinder length
N	Buckling load
R	Cylinder radius
Rm	Mean radius of curvature
t	Cylinder wall thickness
w/t	Imperfection amplitude-to-thickness ratio, manufacturing quality
Y	Yield stress
Z	Batdorf parameter